

# Peripheral mixing of passive scalar at small Reynolds number

G. Boffetta, F. De Lillo

*Dipartimento di Fisica Generale and INFN, Università di Torino, via P.Giuria 1, 10125 Torino (Italy)  
and CNR-ISAC, Sezione di Torino, corso Fiume 4, 10133 Torino (Italy)*

A. Mazzino

*Dipartimento di Fisica, Università di Genova, INFN and CNISM, via Dodecaneso 33, 16146 Genova (Italy)*

(Dated: February 3, 2022)

Mixing of a passive scalar in the peripheral region close to a wall is investigated by means of accurate direct numerical simulations of both a three-dimensional Couette channel flow at low Reynolds numbers and a two-dimensional synthetic flow. In both cases, the resulting phenomenology can be understood in terms of the theory recently developed by Lebedev and Turitsyn [Phys. Rev. E 69, 036301, 2004]. Our results prove the robustness of the identified mechanisms responsible for the persistency of scalar concentration close to the wall with important consequences in completely different fields ranging from microfluidic applications to environmental dispersion modeling.

Mixing of passive tracer in a turbulent flow is a fundamental problem of great technological interest which has undergone a significant theoretical progress in the last years [1, 2]. At low diffusivity and small scales the viscous-convective Batchelor regime of mixing arises for a large value of the Schmidt number  $Sc = \nu/\kappa$ , where  $\nu$  is the kinematic viscosity and  $\kappa$  the molecular diffusivity [3]. In this regime the velocity field can be considered smooth because of the exponential decay of the velocity spectrum. An analogous situation is realized if the tracer is advected by a time dependent, chaotic flow, i.e. a spatially smooth flow at all scales. Several theoretical predictions, including the exponential decay in time of passive scalar fluctuations [4, 5, 6, 7], have been verified in experiments and numerical simulations [8, 9].

Recently, it has been shown that the presence of boundaries can alter significantly the predictions based on an unbounded domain. No slip boundary condition for the velocity field reduces the efficiency of mixing close to the boundary – the peripheral region – which becomes a source of passive scalar. This effect is of particular importance in the case of boundary dominated geometries, such as in microfluidics. Indeed, it is well known that the lack of efficient mixing is one of the problems in many microfluidic devices which operate at vanishing Reynolds number [10]. Several statistical predictions for the peripheral mixing have been recently made [11, 12] and checked with laboratory experiments in a chaotic microchannel [13], in polymer solutions [14] and in kinematic simulations [15].

In this letter, we will discuss the problem of tracer mixing in presence of boundaries by means of direct numerical simulation of a Couette flow at small Reynolds number and in kinematic simulations of a chaotic flow. Before discussing quantitative results, we can have a physical intuition from Figure 1 which shows a snapshot of tracer concentration advected by a two-dimensional chaotic flow. Because of the vanishing velocity, the tracer persists for very long time close to the boundary from

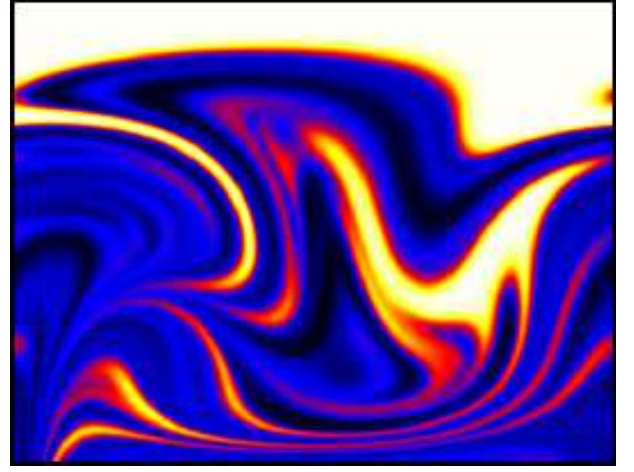


FIG. 1: Snapshot of passive tracer concentration close to a wall placed on the top. White correspond to high concentration, black to low concentration. The initial condition is a step function in the vertical direction. Tracers is advected according to (1) with a two-dimensional synthetic velocity field.

which it is only intermittently transported into the bulk in the form of elongated filaments.

A passive scalar  $\theta$  advected by an incompressible velocity field  $\mathbf{u}$  obeys the equation

$$\frac{\partial \theta}{\partial t} + \mathbf{u} \cdot \nabla \theta = \kappa \nabla^2 \theta \quad (1)$$

where  $\kappa$  is the molecular diffusivity, and appropriate initial and boundary conditions are set for  $\theta$ . In general  $\mathbf{u}$  is subject to its own set of equations, the typical case being Navier-Stokes equations, together with boundary conditions and stirring mechanism which therefore determine the precise form of  $\mathbf{u}$  close to the boundary. However some general predictions on the evolution of  $\theta$  can be made on the basis of the no-slip conditions and incompressibility only, assuming the flow to have a short correlation time with respect to the typical mixing time. To

simplify the notation, but without loss of generality, we assume the flow to be two-dimensional, with  $(x, y)$  the coordinates parallel and normal to the wall ( $y = 0$  corresponding to the wall) and  $(u, v)$  the associated velocity components.

As a consequence of no slip ( $\mathbf{u}(x, y = 0) = 0$ ) and incompressibility ( $\nabla \cdot \mathbf{u} = 0$ ) conditions, there is a region close to the wall, characterized by the scaling  $\langle u^2(y) \rangle \sim y^2$  and  $\langle v^2(y) \rangle \sim y^4$  (where by  $\langle \cdot \rangle$  we indicate the double average with respect to the coordinates parallel to the wall and velocity realizations). The velocities in the bulk of the container or duct are therefore much more intense with respect to the ones in the layers close to the wall, and the passive scalar evolution becomes faster and faster as one moves away from the wall. Starting from these considerations, it is possible to describe the evolution of a passive tracer initially concentrated in a layer of thickness  $\delta$  close to the wall in term of a turbulent diffusivity. Averaging (1), the equation for the  $y$ -evolution of the scalar profile is

$$\partial_t \langle \theta \rangle = \mu \partial_y [y^4 \partial_y \langle \theta \rangle] + \kappa \partial_y^2 \langle \theta \rangle. \quad (2)$$

The first term in the rhs of (2) describes the role of chaotic advection in terms of an eddy diffusivity  $D = \int_0^\infty \langle v(y, 0)v(y, t) \rangle dt \sim \mu y^4$ . Comparison with the second term in the rhs of (2) suggests that the evolution of the profile is dominated by advection as long as  $\delta \gtrsim r_{bl} = (\kappa/\mu)^{1/4}$ , the thickness of the diffusive boundary layer. Under this condition, the diffusive contribution can be neglected and (2) becomes

$$\partial_t \langle \theta \rangle = \mu \partial_y y^4 \partial_y \langle \theta \rangle \quad (3)$$

Taking as initial condition for the scalar a distribution concentrated at the wall with  $\theta(x, 0; 0) = 1$  and  $\lim_{y \rightarrow \infty} \theta(x, y; t) = 0$ , the asymptotic solution of (3) for large times is [12]

$$\langle \theta(y, t) \rangle = \left[ \text{erf} \left( \frac{\delta}{2y} \right) - \frac{\delta}{\sqrt{\pi}y} \exp \left( -\frac{\delta^2}{4y^2} \right) \right] \quad (4)$$

i.e. the profile has a universal form, independently on the details of the initial distribution. The thickness  $\delta = (\mu t)^{-1/2}$  is the only characteristic scale and decreases in time, as the layer occupied by the scalar contracts in the evolution. It is important to remark that the specific form of the profile (4) gives a practically constant concentration for  $y \lesssim \delta/4$ , making the boundary conditions for the scalar irrelevant in the advective stage. We remark that although (1) obviously conserves the average scalar  $\langle \theta \rangle$ , from (4) one has that  $\int \langle \theta(y, t) \rangle dy = \delta(t)/\sqrt{\pi} \simeq t^{-1/2}$  is time dependent. The reason is that in deriving (4) the bulk is considered as an infinite reservoir for the scalar which has therefore zero average.

Neglecting diffusion, the advection equation (1) holds for any local function of  $\theta$  too and therefore its average

is governed by a generalization of (3). In particular the moments of scalar concentration  $\langle \theta^n \rangle$  are expected to follow the same profile (4) independently of  $n$ . This is the mathematical consequence of the intermittent nature of scalar advection shown in Figure 1 in which  $\langle \theta^n \rangle$  is dominated by the white regions in which  $\theta = 1$ . It is also possible to derive an expression for the probability density function valid for any time and distance from the wall as [12]

$$P(\theta, y, t) = \frac{1}{yy_0|\theta'_0(y_0)|} \left[ (1 - 2\mu t y y_0) g \left( \frac{1}{y} - \frac{1}{y_0} \right) + (1 + 2\mu t y y_0) g \left( \frac{1}{y} + \frac{1}{y_0} \right) \right] \quad (5)$$

where  $g(x)$  is a Gaussian distribution with zero mean and variance  $2\mu t$  and the dependence on  $\theta$  is defined implicitly through the monotonic, homogeneous along the wall, initial profile:  $\theta_0(y_0) = \theta$  (note that large  $\theta$  correspond to small  $y_0$ ). At variance with (4), which is valid only asymptotically in time, the prediction for the PDF is valid for any times as it depends on the details of the initial distribution. It is interesting to observe that (5) predicts that  $P(\theta = 1, y, t) = 0$  for any  $y > 0$ : in the absence of diffusion it takes an infinite time for the scalar to be transported away from the wall.

We have tested the above theoretical predictions by means of numerical simulations of a three-dimensional Couette flow and a synthetic two-dimensional flow. For the first case, the Navier-Stokes equations have been numerically integrated in a 3D slab geometry of dimension  $L_x \times 2L_y \times L_z$  with no-slip boundary conditions on the two planes  $y = 0$  and  $y = 2L_y$ , and periodic boundary conditions on the streamwise and spanwise directions  $x$  and  $z$ . The flow is forced by the relative motion of the two opposed walls with opposite velocity  $\pm U_0$ , from which a large scale Reynolds number is defined as  $Re = U_0 L_y / \nu$ . Direct numerical simulations are performed by means of a standard pseudo-spectral Fourier-Chebyshev code [16, 17] at resolution  $128 \times 65 \times 128$  for a domain of size  $L_x \times 2L_y \times L_z = 8 \times 2 \times 8$ . We use a moderate Reynolds number  $Re \simeq 600$ , which is sufficiently large to sustain a turbulent-like motion for long time [18] but still small in order to have a well developed viscous layer where scaling imposed by boundaries is observed. The average wall shear rescaled with mean shear is  $s_0/(U_0/L_y) \simeq 3.3$ , the rescaled friction velocity  $u_*/U_0 = \sqrt{\nu s_0}/U_0 \simeq 0.074$  and the friction Reynolds number  $Re^* \simeq 44$ . Scales and times are made dimensionless with the half-channel height  $L_y$  and large scale time  $T = L_y/U_0$ .

In order to avoid the effects of diffusivity and increase the available observation range, the simulation of the tracer advection (1) was carried out with a Lagrangian method: trajectories of  $N = 10^7$  particles, representing the concentration of tracer, are integrated according to the equation  $\dot{\mathbf{x}}(t) = \mathbf{u}(\mathbf{x}, t)$ . The initial condition for the

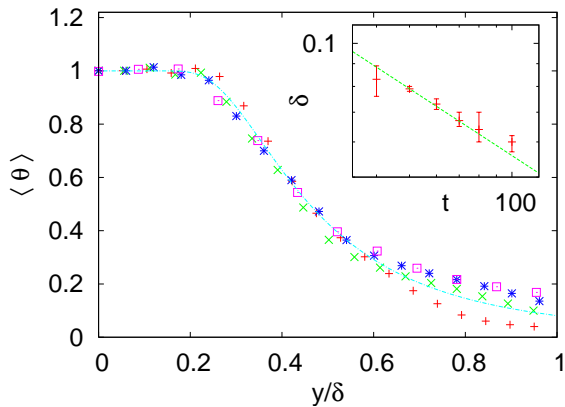


FIG. 2: Profile of the scalar density  $\theta$  at different times in the Couette channel rescaled with respect to  $\delta(t)$  and compared with the theoretical prediction (4) (continuous line). The inset shows the fitted values of  $\delta$  at different times and the prediction  $\delta \simeq t^{-1/2}$ .

particles is an uniform distribution in the  $x$  and  $z$  directions in a layer close to the wall  $y \leq 0.04L_y$ . Continuous tracer distribution  $\theta(\mathbf{x}, t)$  is reconstructed at every time proportional to local tracer density on the grid. The advantage of the present method is the possibility to perform the simulation at Schmidt number virtually infinite (although a small numerical diffusion is always present), at the price of some noise in the reconstruction of small scales due to the discreteness of the tracer.

In Fig. 2 we plot the mean profile  $\langle \theta(y, t) \rangle$  at different times compared with the theoretical curve (4). The value of the thickness  $\delta$  at different time is obtained from the fit of the profiles with (4) and its dependence on  $t$  is compatible with the prediction  $\delta = (\mu t)^{-1/2}$ , from which  $\mu \simeq 3.2$  is estimated.

Figure 2 shows that scalar profiles in the bulk deviate from the theoretical curve at large  $y$ . This is because, even if the value of  $Re$  is small, the  $y^4$  scaling characteristic of the viscous layer, can be observed only up to a distance  $y \sim 0.1L_y$  from the wall. Therefore, in order to extend the range of scaling, we performed an additional set of simulations based on a kinematic model for the velocity field. We define a two-dimensional velocity field in terms of a synthetic stream function  $\Psi(x, y) = \Phi(x, y)G(y)$ , where  $\Phi = \sin(k_x x + \varphi_x(t)) \sin(k_y y + \varphi_y(t))$  represents a time-dependent cellular flow while  $G(y)$  is tailored to reproduce the correct scaling at the wall. If  $G \sim y^2$  for  $y$  close to the wall, the scaling of both components of the velocity is ensured. We chose  $G(y) \simeq [1 - \cos(k_s y)]$  close to each wall, with  $k_s = \pi/(2L_s)$  and the position  $L_s$  of the inflection point defining the width of the scaling region for the velocity,  $y \lesssim L_s$ , which is the region of interest. In the bulk, a matching function connects the profiles. The phases of the cellular flow,  $\varphi_x$  and  $\varphi_y$  are given by a random process with a finite correlation time. The velocity

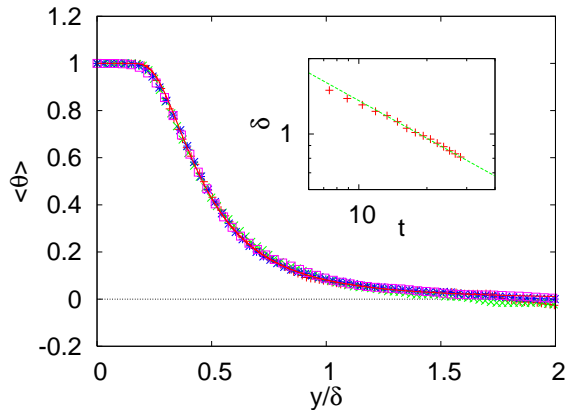


FIG. 3: Average profile of the scalar density  $\theta$  at different times rescaled with respect to  $\delta$  and the bulk average  $b$  (see text) and compared with (4) (continuous line). In the inset, the thickness of the profile is shown together with the prediction  $t^{-1/2}$  dependence.

field generated by  $\Phi$  is placed on a grid of size  $L_x = \pi$  and  $2L_y = 4\pi$  at resolution  $512 \times 2048$  where the evolution of (1) is integrated by means of a pseudo-spectral code, with periodic boundary conditions. This numerical approach is similar to that used in [15, 19]. Scaling regions extend approximatively to  $L_s = 4$ . The time unit is chosen so that the correlation time of the velocity field is  $T = 1$ . In these units we have  $\mu \simeq 2.66$  and  $\kappa = 3.42 \times 10^{-6}$  and therefore the width of the diffusive boundary layer is  $r_{bl} \simeq 0.034L_y$ . As initial condition we choose a distribution null in the bulk and concentrated at the walls in two smoothed-step functions of size  $L_y/4$ . The results are based on ensemble average over 100 realizations of the random noise driving the kinematic velocity field.

In Fig. 3 the profile  $\langle \theta(y, t) \rangle$  is compared, at different times, with the theoretical curve. In order to accurately resolve the region close to the wall, the extension of the domain in the bulk is not large enough for the approximation of an infinite bulk to be valid. Therefore, because of the conservation of  $\langle \theta \rangle$ , after a short transient a relevant amount of scalar accumulates in the central region of the domain, thus affecting the overall shape of the profile. In order to compare the numerical results with the theoretical prediction based on an infinite basin, we computed the profile of the auxiliary field  $\tilde{\theta} = (\theta - b)/(1 - b)$ , where  $b(t)$  is the time-dependent value of  $\theta$  in the bulk (averaged over  $x$ ). Figure 3 shows the remarkable agreement obtained between theory and numerics, indicating that the profile (4) can be easily extended to the general case of advection in a finite vessel. From the fitting procedure we get the values of the parameter  $\delta$ , which is found to follow accurately the prediction  $\delta(t) = (\mu t)^{-1/2}$  with  $\mu \simeq 2.13$  (see inset of Fig. 3).

Figure 4 shows the profiles of different moments of scalar concentration  $\langle \theta^n(y, t) \rangle$  computed at an interme-

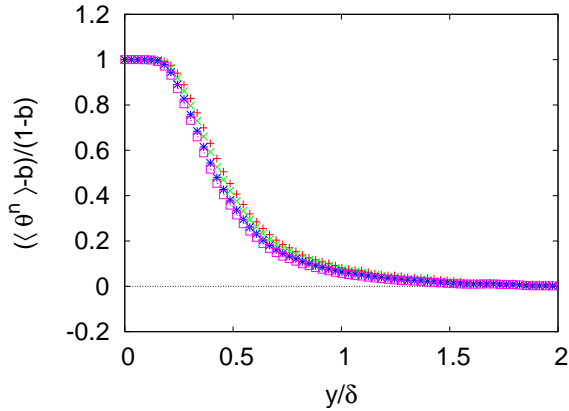


FIG. 4: Average profiles of moments of scalar density  $\langle \theta^n \rangle$  for  $n = 1$  (+),  $n = 2$  (x),  $n = 4$  (\*) and  $n = 6$  (□) at time  $t = 18T$  in the two-dimensional kinematic simulation.

diate time. All the moments collapse on the prediction (4), confirming the fact that in this stage diffusion is negligible and mixing of the scalar is dominated by eddy diffusivity according to (3).

We have also computed the probability density function,  $P(\theta, t, y)$ , of the passive scalar. The results, at a distance  $y = L_y/4$  from the wall, corresponding to the thickness of the initial distribution, are shown in Fig. 5 for two different times. At very short time the PDF is peaked around the initial condition  $\vartheta_0/2$ . Observe that the distribution is much more narrow than that theoretically predicted by (5), because the eddy diffusivity approximation (2) is not justified at short times.

At longer time the PDF forms two pronounced peaks at the extreme values which are responsible for the saturation of the moments of  $\theta$ , since the peak in  $\theta = 1$  gives a dominant contribution to any  $\langle \theta^n \rangle$ . Physically the presence of the two peaks is related to long tongues protruding from the wall region into the bulk. Advection stretches such structures, while preserving the value of  $\theta$ , the smoothing effect of molecular diffusivity becoming effective only on longer times.

In conclusion, our results for both the three-dimensional channel flow and the two-dimensional synthetic flow are accurately explained by the theoretical description of Ref. [12]. Our results emphasize the importance of a correct description of the close-to-the-wall region where a scalar field tends to persist. The incorrect reproduction of near-wall scaling behavior  $u(y) \propto y$  and  $v(y) \propto y^2$  necessarily destroys the above mechanism. This might be a serious problem in applications of environmental dispersion modeling under strong stability conditions where the viscous layer can reach values of orders of meters thus affecting the realm of human activities. A poor (in term of resolution) description of this region would result in a dangerous underestimation of the level of pollutants concentration close to the ground.

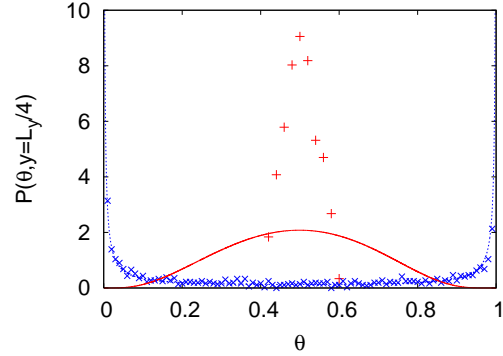


FIG. 5: PDF's of the scalar density in the kinematic simulation at  $y = L_y/4$ , corresponding to the thickness of the initial distribution at times  $t = 0.02$  (+) and  $t = 3.0$  (x). Lines show theoretical predictions.

This work was supported by Piedmont Industrial Research Grant INUMICRO.

- 
- [1] B. Shraiman and E. Siggia, *Nature* **405**, 639 (2000).
  - [2] G. Falkovich, K. Gawędzki, and M. Vergassola, *Rev. Mod. Phys.* **73**, 913 (2001).
  - [3] G. K. Batchelor, *J. Fluid Mech* **5**, 113 (1959).
  - [4] R. T. Pierrehumbert, *Chaos Solitons Fractals* **4**, 1091 (1994).
  - [5] D. T. Son, *Phys. Rev. E* **59**, R3811 (1999).
  - [6] E. Balkovsky and A. Fouxon, *Phys. Rev. E* **60**, 4164 (1999).
  - [7] P. Haynes and J. Vanneste, *Physics of Fluids* **17**, 097103 (2005).
  - [8] A. Groisman and V. Steinberg, *Nature* **410**, 905 (2001).
  - [9] B. Williams, D. Marteau, and J. Gollub, *Physics of Fluids* **9** (1997).
  - [10] T. M. Squires and S. R. Quake, *Rev. Mod. Phys.* **77**, 977 (2005).
  - [11] M. Chertkov and V. Lebedev, *Phys. Rev. Lett.* **90**, 034501 (2003).
  - [12] V. V. Lebedev and K. S. Turitsyn, *Phys. Rev. E* **69**, 036301 (2004).
  - [13] C. Simonnet and A. Groisman, *Phys. Rev. Lett.* **94**, 134501 (2005).
  - [14] T. Burghel, E. Segre, and V. Steinberg, *Phys. Rev. Lett.* **96**, 214502 (2006).
  - [15] H. Salman and P. H. Haynes, *Phys. Fluids* **19**, 067101 (2007).
  - [16] C. Canuto, M. Hussaini, A. Quarteroni, and T. Zang, *Spectral methods in fluid dynamics* (Springer-Verlag New York, 1988).
  - [17] F. De Lillo and B. Eckhardt, *Physical Review E* **76**, 16301 (2007).
  - [18] S. Malerud, K. Måløy, and W. Goldburg, *Physics of Fluids* **7**, 1949 (1995).
  - [19] A. Chernykh and V. Lebedev, *JETP Letters* **87**, 682 (2008).